Hepatitis E virus replication is facilitated by epithelial cell turnover and targets enteroendocrine cells in human intestinal organoids

Nanci Santos-Ferreira[1*], Xin Zhang[1*], Jana Van Dycke[1], Johan Neyts[1], Suzanne Kaptein[1], Joana Rocha-Pereira[1]

[1]KU Leuven-Department of Microbiology, Immunology and Transplantation, Rega Institute, Laboratory of Virology and Chemotherapy, Leuven, Belgium

Corresponding author(s). E-mail(s): suzanne.kaptein@kuleuven.be, joana.rochapereira@kuleuven.be

*These authors contributed equally to this work.

Keywords

Hepatitis E virus; Human intestinal enteroids; infection; stem cells; Enteroendocrine cells; virus-host interactions

Abstract

Hepatitis E virus (HEV) is an emerging pathogen responsible for acute viral hepatitis globally. There is no specific antiviral and non-universal vaccine, partly due to limitations in its *in vitro* cultivation. Although HEV is mainly fecal-oral transmitted and excreted in the feces in high titers, the role of the gut in HEV-induced disease remains unexplored. Little is known about how the virus spreads from gut to liver, or about the gut potentially acting as an HEV reservoir. To address this, we developed an HEV infection model using human intestinal enteroids (HIEs). HEV infection was done using: a) differentiated 3D-HIEs; b) differentiated 2D-HIEs in transwells; c) electroporation of HIEs with HEV capped RNA. 3D infection with HEV-3 strains resulted in a limited increase in HEV RNA. Infection of 2D-HIEs yielded similar replication levels, with shedding mainly to the apical side of the intestinal epithelial layer. Importantly, electroporation of HIEs with HEV-3 RNA resulted in a sustained increase in viral load over time in the supernatant, with the detection of infectious virus particles. Likewise, electroporation of HEV-1 and 3 luciferase replicon RNA, a 5-fold and 20-fold increase in luciferase signal was observed. Treatment with the current off-label ribavirin effectively inhibited viral replication in the luciferase subgenomic or full-length genomic HEV RNA electroporated HIEs.

Moreover, here we investigate the cellular tropism of hepatitis E virus in HIEs. Abundant HEV ORF2 antigen was detected in infected HIEs, including proliferating cells, enterocytes and enteroendocrine cells, with increased mRNA expression for the latter cell type. Overall, we here established a model for HEV infection in HIEs and discovered that the fast cell turnover of the intestine is an important feature that enables efficient HEV replication. Furthermore, HEV infection promotes differentiation towards enteroendocrine cells, which the virus can infect.

Introduction

The enteric hepatitis E virus (HEV) poses a substantial global health burden. It is mainly transmitted through the fecal-oral route, with strains causing human infection predominantly belonging to the *Paslahepevirus balayani* species of the *Hepeviridae* family[1]. HEV-1 and HEV-2 are endemic in developing regions and are mainly transmitted via contaminated drinking water, with an estimated 70,000 deaths annually[2,3]. HEV-1 and 2 occasionally result in fulminant hepatitis with an overall mortality rate of 0.5 to 4%, but with an even higher risk of 20 to 30% in pregnant women[4]. HEV-3 and HEV-4, on the other hand, are zoonotic viruses infecting swine, deer and wild boar and are transmitted via contaminated animal products (*e.g.* raw or undercooked meat products), resulting in sporadic autochthonous infections in both developing and industrialized regions[2]. Extra-hepatic manifestations are often described, affecting mostly the kidney, and the neurological and hematological system[5]. HEV-3 can also lead to chronic infections, especially in immunocompromised individuals, resulting in an increased risk for rapid progression to cirrhosis, graft loss and death[6]. Moreover, HEV is an emerging potential threat to blood safety in industrialized countries after the documentation of several cases of transmission by HEV-contaminated blood, blood products, or by transplantations[7]. There is currently no widely available vaccine or approved specific antiviral therapy. The broad-spectrum antiviral ribavirin is used off-label to treat the chronically infected patients, but is associated with marked adverse effects and treatment failure[8–10].

Many knowledge gaps still remain on fundamental aspects of HEV infection and disease, partly due to difficulties in its cultivation. HEV *in vitro* cultivation in liver-derived primary cells and immortalized cell lines is often used despite its slow replication to low titers. Recent progress involving the generation of cDNA clones and passaging primary patient isolates in distinct cell lines has improved *in vitro* HEV propagation[11]. Nonetheless, new and improved models are needed to replicate the full tropism of HEV.

HEV is a positive-sense single-stranded RNA virus with an icosahedral capsid[12]. Infected hosts produce two types of HEV virions, quasi-enveloped particles (HEV env^+) and naked/non-enveloped particles (HEV env^-). In infected patients or animals, HEV env^+ is released from the apical membrane into the bile duct, where the lipid envelope is degraded by detergents and proteases in the bile, resulting in the presence of HEV env^- in feces and bile[13]. This is presumed to be the main form responsible for

transmission and associated with higher infectivity[14,15] In cell culture, intracellular HEV is predominantly HEV env^-, while membrane associated HEV env^+ is secreted into the supernatant and circulates in blood[16].

Despite the fact that HEV is an enteric virus transmitted fecal-orally and shed in high titers in the stool[12], little attention has been given thus far to the role and contribution of the gut compartment in HEV-induced disease. Evidence that HEV effectively replicates in intestinal epithelial cells was recently brought forward[17]. HEV was found to produce infectious particles that are released from both the basal and apical sides of polarized primary enterocytes, with preferential apical release. Moreover, ribavirin failed to block viral secretion into the apical side, possibly explaining viral relapses in chronic infected patients. Here, authors postulated that the gut epithelium is the initial site of virus amplification before dissemination to the liver, and a reservoir for replicating HEV, especially during chronic infections. Still, viral dissemination strategies between the gut and liver remain poorly understood, and in what way the gut functions as an HEV reservoir is unknown. Moreover, a detailed understanding of HEV infection in the intestine is still lacking, namely regarding the specific intestinal cell types that are infected, their host response upon infection, the viral dissemination strategies to extra-intestinal tissues and disease-inducing mechanisms.

The development of organoid technology provides the opportunity to advance knowledge in virus biology and host-pathogen interactions to a much higher level of physiological relevance and thus is/will be revolutionary in many fields of biomedical research, including drug discovery. Indeed, HEV replication in human liver-derived organoids has been reported[18]. Human intestinal organoids are the closest model to mimic the human intestinal epithelium *in vitro* and have been used to dissect virus-host interaction of several viruses, such as noroviruses[19], rotaviruses[20], astroviruses[21], adenoviruses[22], enteroviruses[23] and coronaviruses. Intestinal organoids are non-transformed three- dimensional (3D) cell cultures arranged in a crypt-villus structure that incorporate the physiological features of the intestinal epithelium, including the presence of different cell populations (enterocytes, goblet cells, enteroendocrine and Paneth cells). Self-renewal of the small intestinal epithelium is driven by the proliferation of intestinal stem cells and their progenitors located in the crypts. These stem cells move along different molecular gradients from the bottom of the crypt to the villi domain, resulting in an increasing maturation of specialized cell types[24]. Intestinal organoids can be produced from pluripotent stem cells (iPSCs) or derived from tissue

119 containing Lgr5+ stem cells, better known as human intestinal enteroids (HIEs)[25,26].
120 We here used HIEs to establish an HEV infection model of the small intestine using
121 various formats, with the aim of studying the infection dynamics and characterizing the
122 cellular tropism of hepatitis E virus in the human intestine.
123

124 **Results**

125 **Infection of differentiated 3D human intestinal enteroids with HEV**

126 To investigate whether HIEs are permissive to HEV replication, infection of adult and
127 fetal HIEs was performed using 3D-HIEs after 5 days of differentiation, as previously
128 described[27,28]. Infection of differentiated 3D-HIEs was performed in suspension with
129 Kernow-C1 p6 or Kernow-C1 p6 G1634R (i.e. bearing a fitness enhancing mutation[8]),
130 after which viral load (derived from pooled cell extracts and supernatant) was
131 assessed at different days post-infection (pi) (Fig. 1A). Even with an inoculum of 1.0 ×
132 10^7 HEV RNA copies, infection with Kernow-C1 p6 of either adult or fetal HIEs resulted
133 in a very limited gain in HEV RNA over input (Fig. 1B). Infection with 5.0 × 10^7 RNA
134 copies of Kernow-C1 p6 G1634R yielded a modest increase of ~1 $\log_{10}$ in HEV RNA
135 from 6 to 24 hours pi, after which levels remained stable until the end of the experiment
136 at 5 days pi (Fig.1C). This shows that a high inoculum is required to kick-start infection.
137 Given that HEV is a slowly replicating virus, prolonging the assay past 5 days pi would
138 likely favor replication. However, this was not feasible due to the differentiated state of
139 the cells and the consequent accumulation of debris in the lumen of the 3D organoid
140 structure, resulting in loss of viability past that timepoint. Supplementation with the bile
141 acid glycochenodeoxycholic acid (GCDCA) together with ruxolitinib was attempted,
142 which was previously shown to facilitate the replication of other enteric viruses[27],
143 yielded no obvious benefit (Fig. S1).

144

145 **Infection of HIE polarized monolayers with HEV**

146 Next, we cultured HIEs as polarized monolayers (2D) in a transwell system, thus
147 allowing us to study virus shedding into the apical and basolateral compartments (Fig.
148 2A). Before HEV infection, we determined the transepithelial electrical resistance
149 (TEER) of the monolayers to be > 300 Ω/cm^2. Infection of differentiated fetal and adult
150 2D-HIEs (Fig. 2B and 2C) with Kernow-C1 p6 G1634R yielded a constant virus
151 shedding (HEV RNA levels were ~ 5.5 $\log_{10}$/mL) to the apical side of the intestinal
152 epithelial layer. Basolateral shedding was also detected, albeit at lower levels of ~ 3.5
153 - 4 $\log_{10}$ HEV RNA copies/mL from day 1 to 7 pi. Considering that every 2 days, half
154 of the culture media was replaced by fresh media in both compartments, this indicates
155 a considerable amount of new virions were being produced and shed into the cultures
156 supernatant. Intracellularly, HEV RNA levels detected were approximately 5 $\log_{10}$
157 copies/well (Fig. 2C).

158

159 **Efficient electroporation of HIEs with HEV capped RNA**

160 We next evaluated whether electroporation of a HIE single-cell suspension was
161 feasible and would result in more efficient HEV replication. Given that electroporation
162 of fully differentiated HIEs resulted in non-viable cells, undifferentiated HIEs were used
163 instead, which were electroporated with subgenomic or full-length HEV capped RNA
164 from human HEV-1 (Sar55/S17), HEV-3 (Kernow-C1 p6 or Kernow-C1 p6 G1634R),
165 and rat HEV (pLA-B350), as illustrated in Fig. 3A. For electroporation experiments,
166 3D-HIEs were first dissociated into single cells. Previous reports, showed that adding
167 a rho-associated protein kinase (ROCK) inhibitor and replacement of Wnt activators
168 with a glycogen synthase kinase 3 (GSK-3) inhibitor enhanced the recovery of single
169 cells[29,30] that otherwise fail to replicate sufficiently, primary due to anoikis[29]. HIEs were
170 therefore pre-treated with Y-27632 (ROCK inhibitor) and CHIRR99021 (GSK-3
171 inhibitor) in OGM for 2 days prior to electroporation. The cultures were substantially
172 composed of intestinal stem cells that continue to proliferate and constitute 3D
173 structures.

174 HIEs electroporated with HEV subgenomic RNA of HEV-3 Kernow-C1 p6/luc or HEV-
175 1 Sar55/S17/luc yielded a 20-fold or 5-fold higher luciferase signal, respectively, at 11
176 days post-electroporation (pe) (Fig. 3B). By contrast, electroporation with rat HEV pLA-
177 B350 resulted in 1-2 $\log_{10}$ lower luciferase levels, which may be due to the fact that
178 this is not a human virus or to the absence of the replication-enhancing human
179 ribosomal protein S17 in the viral genome[31]. Treatment with ribavirin resulted in lower
180 luciferase signals when compared to non-treated control, with an half-maximum
181 concentration between 25 and 50 μM (Fig. 3C). Electroporation with full length
182 Kernow-C1 p6 or Kernow-C1 p6 G1634R resulted in a sustained increase in viral load
183 in the supernatant over time, reaching 3.1×10^5 and 5.5×10^5 HEV RNA copies/mL,
184 respectively, at 11 days pe (Fig. 3D). Treatment of full length Kernow-C1 p6 G1634R
185 electroporated HIEs with ribavirin resulted in a dose-dependent reduction of
186 intracellular and extracellular HEV levels (Fig. 3E).

187 Light microscopy of electroporated HIEs shows that they continued to proliferate
188 during the experiment, forming the characteristic 3D structures (Fig. 3F).
189 Immunostaining showed a marked presence of viral antigens (ORF2) in HIEs
190 electroporated with Kernow-C1 p6 or Kernow-C1 p6 G1634R at 15 days pe (Fig. 3G).
191 However, HIEs electroporated with HEV appeared to be smaller than the mock-

192 electroporated ones (Fig. 3F), which is likely not due to cell death since HEV-
193 electroporated HIEs presented less propidium iodide staining (indicative of intact cell
194 membranes), than mock-infected (Fig. S2). HEV replication thus appears to slow down
195 HIE proliferation.
196 More importantly, we confirm that Kernow-C1 p6 G1634R electroporated HIEs
197 produce HEV infectious particles as evidenced by the expression of HEV ORF2
198 antigens on day 7 pi in HepG2/C3A cells that were infected with supernatants from
199 electroporated HIEs (collected on 11 days pe, Fig. S3), resulting in a titer of 3.0×10^7
200 focus forming units (FFU)/mL. Overall, electroporation of HIEs with HEV capped RNA
201 allowed more efficient HEV replication, alike with what is reported in human
202 hepatocytes[15].
203
204 **Infection of undifferentiated 3D- or 2D-HIEs does not improve HEV replication**
205 We next wondered whether the enhanced HEV replication upon electroporation could
206 be due to the use of undifferentiated HIEs. Hence, we repeated the HEV infection
207 experiment using 3D-HIEs and 2D-HIEs (transwell). However, a subset of the HIEs
208 was not treated with differentiation media (ODM) but instead only with growth media
209 (OGM), thereby retaining the stem cell niche and associated proliferation capacity.
210 Infection of undifferentiated 3D-HIEs with HEV Kernow-C1 p6 G1634R yielded a more
211 efficient first replication cycle (8.0×10^3 RNA copies in OGM versus 3.3×10^3 RNA
212 copies in ODM) at 1 day pi (Fig. 4A) but resulted in similar viral loads overtime as in
213 differentiated 3D-HIEs. Moreover, viral load remained more or less constant up to 10
214 days pi, even when half medium was changed every 2 days (from 4 days pi).
215 Infection of undifferentiated 2D-HIEs in transwell resulted in a continuous apical
216 release of virus (Fig. 4B and 4C). Importantly, despite being infected with the same
217 input (2.0×10^8 copies), virus attachment (and likely entry) was less efficient in
218 undifferentiated 2D-HIEs compared to differentiated 2D-HIEs, resulting in lower levels
219 of viral RNA being detected intra and extracellularly (Fig. 2B-C and Fig. 4B-C). In
220 summary, the differentiation state of the HIEs at the start of infection does not seem to
221 play a critical role in supporting HEV replication (at least not alone).
222
223 **HEV infection induces HIE differentiation into mature cell lineages**
224 Since viral infections might affect intestinal cell differentiation, we next investigated the
225 differentiation state of electroporated HIEs at the end of the experiments (hence 11

226 days pe), by comparing it to day 0 pe cultures using gene expression analysis (Fig. 5).
227 Comparison of mRNA levels of Lgr5 (stem cells), lysozyme (Paneth cells), sucrose
228 isomaltase (mature enterocytes), mucin 2 (goblet cells) and chromogranin A
229 (enteroendocrine cells), revealed that Kernow-C1 p6 G1634R induces expression of
230 mature cell types, mainly enterocytes and enteroendocrine cells. However, infection
231 with Kernow-C1 p6 resulted in the reduction of the expression of intestinal stem cells
232 (Lgr5+), with similar transcript levels of the other cells types compared to mock-
233 electroporated HIEs.
234
235 **HEV shows tropism to proliferating and mature intestinal cells**
236 We next investigated which intestinal cell lineages are permissive to HEV replication.
237 To that end, we performed confocal imaging of immunostainings with virus marker and
238 cell markers of HIEs electroporated with HEV Kernow-C1 p6 or p6 G1634R at the peak
239 of viral replication, *e.g.* 11 days pe (Fig. 6). This revealed that proliferating cells, *e.g.*
240 positive for Ki67 (proliferation marker), are positive for HEV ORF2 protein (Fig. 6A and
241 Fig. S4, as indicated by the white arrows). Due to Ki67 labelling the cell nuclei, while
242 HEV localizes to the cytoplasm, determining their colocalization based on intensity is
243 not feasible. Likewise, most enterocyte-specific antibodies (*e.g*. SI - sucrose
244 isomaltase) stain the apical surface thus making colocalization studies challenging.
245 However, enterocytes are the major cell type of the intestinal epithelium and infected
246 HIEs show a broad and extensive signal of ORF2 hinting that enterocytes are most
247 likely infected (Fig. 6B). Importantly, HEV ORF2 signal was also found in
248 enteroendocrine cells (CHGA – chromogranin A) (Fig. 6C and Fig. S5, as indicated by
249 the white arrows). Colocalization of virus with chromogranin A showed that 2.2% of the
250 thresholded capsid protein ORF2 signal colocalized with enteroendocrine cell marker,
251 while 21.7% of the thresholded enteroendocrine cells signal overlapped with ORF2
252 signal (Pearson coefficient of 0.328). Moreover, HIEs containing a high amount of
253 mucins (WGA – wheat germ agglutinin), produced by goblet cells, have less virus (Fig.
254 6D). Colocalization analysis showed that 9.1% of the thresholded capsid protein ORF2
255 signal colocalized with mucus-producing goblet cells (based on mucin staining), while
256 2.4% of the thresholded goblet cells signal overlapped with ORF2 signal (Pearson
257 coefficient of -0.056). Overall, HEV ORF2 capsid protein is present in both proliferating
258 and mature cells.

Discussion

Hepatitis E virus has been recognized as enterically transmitted since the last century[32], yet evidence supporting its infection in the gastrointestinal tract has remained limited, which partly due to relatively inefficient *in vitro* cultivation. Understanding HEV infection in the primary infection site, the intestine, as well as HEV dissemination to the liver is essential to grasp its pathogenesis. Additionally, identifying the intestinal cellular tropism of HEV will offer novel insights into virus-host interactions and potential disease mechanisms, all of which is very relevant for the development of therapeutics. The advent of the organoid technology has revolutionized the *in vitro* culture of several enteric viruses, enabling us to study some of them for the first time. This holds great promise also for HEV, which is regarded a slow hard-to-cultivate virus. While organoid cultures are complex and demanding, they are also flexible and incredibly powerful since they can be of iPSC- or tissue-derived origin, from different organ segments, from donors of different ages, sex and ethnicity thus enabling us to achieve a much more realistic view of host and disease.

There are several methods to deliver infectious organisms into organoid cultures[33]. We here established three different setups for HEV infection in HIE cultures. First, 3D-HIEs were mechanically disrupted into fragments and incubated with HEV. The fragments reassemble into intact organoids containing the pathogens within the lumen. Second, HIEs were enzymatically disrupted into single cells and seeded in transwell membranes forming 2D monolayers that offer easy access to the apical side of the epithelium, which can be used for HEV infection. Third, electroporation of undifferentiated HIE single cells with *in vitro*–transcribed HEV RNA was performed.

HEV Kernow-C1 p6 and p6 G1634R were able to replicate in fetal or adult differentiated 3D-HIEs in an input dependent-manner. However, replication was somewhat limited, with a constant viral load detected up to 5 days pi. Furthermore, adding ruxolitinib (a selective inhibitor of JAK1 and JAK2[34]) or GCDCA (required for efficient replication for other enteric virus[35]), to the infection medium had no significant impact on Kernow-C1 p6 G1634R replication in 3D-HIEs. The same was observed when infecting 2D-differentiated HIE monolayers in transwell, showing that access to the apical surface was not the limitation for inefficient replication in 3D-HIEs. 2D-HIE infection mainly resulted in apical release of HEV: basolateral shedding was ~ 2 $\log_{10}$ lower. These data, in line with previously described results in primary intestinal

292 epithelial cells[17], suggests that new HEV virions can be continuously excreted into the
293 lumen. This supports the idea that the intestine functions as a reservoir for HEV.
294 Electroporation of HIE single cell suspensions with HEV capped RNA was the most
295 effective approach for exploring HEV infection in the gut, resulting in continuous and
296 steady viral replication overtime with either full-length or replicon HEV RNA.
297 Productive infection was further confirmed by the detection of infectious virus particles
298 in the culture supernatant. In addition, the model was amenable to antiviral studies to
299 evaluate the efficacy of new therapeutic approaches in the intestinal compartment.
300 Importantly, previous work on primary intestinal cells highlighted that a multi-organ
301 view on HEV infection of the host may be the key to understanding the failure of
302 ribavirin treatment (or of yet-to-be developed treatments) in some patients[17]. Here, we
303 validated our infection model by showing that ribavirin reduced the viral RNA levels
304 both intra- and extracellularly in a dose-dependent manner in the HEV-electroporated
305 HIEs.
306 Given that upon electroporation, HIE cells are in a proliferative state, we assessed
307 whether the use of undifferentiated HIEs, either in 3D or 2D, would result in better viral
308 yields, comparable to electroporation. However, the outcome of this infection was alike
309 what was obtained with differentiated HIEs, hinting that HEV does not have a strong
310 preference for undifferentiated cells. Starting HEV infection from undifferentiated
311 populations does offer the opportunity to prolong assays (given differentiated cells stay
312 viable for less days), which may allow additional HEV replication over time. Yet, there
313 was no obvious advantage in 3D-HIEs or 2D-HIEs. Other factors likely play a role in
314 the replication and/ or further dissemination of the virus. An obvious one is that
315 electroporation overcomes the early replicative steps of entry and uncoating. However,
316 the fact that a truly exponential increase in viral load is only apparent 3 days after
317 electroporation hints that the advantage is perhaps related to cell multiplication (which
318 is a slower process). If viral entry would be the main bottleneck, a strong and steady
319 increase in virus yield would be detected as early as 1 day pe. Moreover, HEV
320 sustained viral load over time, despite frequent medium changes, indicates HEV is a
321 slow growing virus in intestinal cells, a feature we see in hepatocyte-like immortalized
322 models, primary hepatocytes[15] and liver organoids[18].
323 Up to now, the cell tropism of HEV in the intestinal epithelium has not been described.
324 Confocal microscopy of HEV electroporated HIEs stained with an HEV ORF2-specific
325 polyclonal antibody showed the presence of abundant viral capsid antigen in

326 proliferating cells, enteroendocrine cells, and most likely enterocytes. Enteroendocrine
327 cells are estimated to comprise approximately 1% of the intestinal epithelial cell
328 population, while enterocytes are the major intestinal cell type[36]. Infected HIEs show
329 a broad and extensive signal of ORF2 suggesting enterocytes are infected.
330 Furthermore, the gene expression data suggests that HEV infection promotes cell
331 differentiation without affecting or even suppressing (Kernow-p6) the proliferation
332 niche. In light of these findings, we hypothesize that HEV infection directly benefits
333 from the fast cellular turnover of the intestinal crypt/ villi and its constant proliferation
334 and maturation. In fact, the virus appears to, on one hand infect proliferating cells and
335 on the other hand, promote and direct cell maturation in the direction of desired
336 lineages, particularly in the case of enteroendocrine cells. Further analysis is
337 necessary to determine precisely how does the virus benefit from this process and
338 what advantages may infecting enteroendocrine cells bring. Conversely, mucus-
339 producing goblet cells seem to have mainly a protective role against HEV, given their
340 absence of colocalization with the virus. Further investigations could determine how
341 HEV infection affects mucus production, as a part of the host response to infection.
342 An equally important future step will be to determine which HEV particles are produced
343 in HIEs, *e.g.* naked or quasi-enveloped virions, as HEV infectivity has mostly been
344 determined in hepatocyte-like models, showing HEV env^- virions are more infectious.
345 Overall, we here established a model for HEV infection in HIEs and discovered that
346 the fast cell turnover of the intestine is an important feature that enables efficient HEV
347 replication. Moreover, we discovered that HEV infection promotes differentiation
348 towards enteroendocrine cells, which the virus can infect. The use of intestinal
349 organoids will contribute to much deeper understanding of HEV infection and disease.

350 **Material and Methods**

351 **Cells and enteroids culture**

352 HepG2/C3A cells (ATCC CRL-10741) were cultivated in DMEM, supplemented with
353 10% FBS, 2 mM L-glutamine, 0.75 g/L sodium bicarbonate (Gibco) and 1 mM sodium
354 pyruvate (Gibco).
355 The experimental plate for HepG2/C3A cells was prepared by coating with 100 µg/mL
356 of rat tail collagen (Sigma-Aldrich) and 0.02 M glacial acetic acid in PBS for a minimum
357 of 2h at 37°C. Subsequently, the plates were washed three times with PBS.
358 Human intestinal enteroids derived from fetal ileum (HT124), adult jejunum (J2) and
359 adult small intestine (Lonza), were maintained at 37°C with 5% CO_2 in extracellular
360 matrix (Matrigel, Corning, 354234) and IntestiCult™ Organoid Growth Medium (OGM,
361 StemCell Technologies), that was replaced every other day. Differentiation was
362 triggered by Wnt3a removal with IntestiCult™ Organoid Differentiation Medium (ODM,
363 StemCell Technologies) for 5 days with medium changes every other day.
364

365 **Viruses and generation of infectious virus stocks**

366 Genotype 3 full-length Kernow-C1 p6 infectious cDNA clone (GenBank accession
367 number JQ679013) and its G1634R variant, containing the G1634R mutation in the
368 viral polymerase, were previously detailed[8]. The subgenomic Kernow-C1 p6/luc, which
369 partial of ORF2 was replaced by the *Gaussia* luciferase gene, was constructed as
370 described previously[31]. Similarly, the genotype 1 reporter replicon Sar55/S17/luc was
371 derived from the HEV strain Sar55/S17 (GenBank accession number AF444002), as
372 described earlier[37]. Plasmids Kernow-C1 p6, Kernow-C1 p6/luc, and Sar55/S17/luc,
373 were kind gifts provided by Prof. Suzanne Emerson (formerly at the National Institute
374 of Allergy and Infectious Diseases, National Institutes of Health, Bethesda, MD, USA).
375 The construction of plasmid pLA-B350/luc was previously mentioned[38].
376 Capped viral RNA was generated from the cDNA plasmids as previously described[10].
377 In brief, Kernow-C1 p6, Kernow-C1 p6 G1634R, Kernow-C1 p6/luc, and pLA-B350/luc
378 were linearized by MluI, Sar55/S17/luc was linearized by BglII. Subsequently, *in vitro*
379 transcription was carried out using the Ribomax large-scale RNA production systems
380 from Promega, and capping using the ScriptCap m7G capping system (Cellscript).
381 Kernow-C1 p6 or G1634R virus stocks were the mixture of non-enveloped and
382 enveloped virus ($env^{+/-}$) or only non-enveloped virus (env^{-})[15,39]. In short, capped
383 Kernow-C1 p6 or G1634R RNA was transfected into HepG2/C3A cells through

384 electroporation as previously described[15,39]. After seven days of incubation,
385 extracellular enveloped and intracellular non-enveloped Kernow-C1 p6 or G1634R
386 were harvested as follows. To harvest the virus from extracellular, supernatant was
387 collected and centrifuged at 4,000 rpm at 4°C for 15 min, after remove the cell debris,
388 the supernatant was concentrated around 10 times by using minimate tangential flow
389 filtration capsules (100K pore size, Pall Corporation).
390 For intracellular virus harvesting, collect the electroporated cells by trypsinization,
391 resuspended the cells in fresh complete DMEM, and release the virus from cells by
392 three freeze-thaw cycles in the liquid nitrogen. The lysate was subsequently
393 centrifuged at 10,000 x*g* for 10 min. Concentrated enveloped virus were mixed with
394 non-enveloped virus, or non-enveloped virus, aliquoted, and stored at -80°C. To
395 evaluate the infectious virus titer and viral RNA level of the stock, immunofluorescence
396 staining of the HEV ORF2 protein and RT-qPCR were conducted, as previously
397 described[15].
398
399 **HEV infection in 3D enteroids**
400 HEV infection of 3D-HIEs was performed as previously describe for other enteric
401 viruses with minor modifications[23,27,28]. Briefly, 3D-HIEs were removed from matrigel,
402 thoroughly washed with CMGF (-) medium (Advanced DMEM/F12 supplemented with
403 GlutaMAX-1 2 mM (Gibco), HEPES 10 mM (Gibco), penicilin-streptomicin 100 U/mL
404 (Gibco) and primocin 100 µg/mL (Invivogen), and gently fragmented. 3D-HIEs were
405 resuspended in infection medium (ODM supplemented with 500 µM
406 glycochenodeoxycholic acid (GCDCA; Sigma-Aldrich) and 10 µM Y-27632 (StemCell
407 Technologies) and inoculated with HEV or mock infected. After virus inoculation, 3D-
408 HIEs were incubated for 6h at 37°C with homogenization every hour. After, 3D-HIEs
409 were washed with CMGF(-) (5 x), resuspended in matrigel and plated in pre-warmed
410 48-well plates (20 µL drop containing 1.0×10^5 cells). After matrigel polymerization for
411 10 min at 37°C, infection media (ODM supplemented with 500 µM GCDCA and 10 µM
412 Y-27632 and 2 mM ruxolitinib (Toronto Research Chemicals) was added to each well.
413 At multiple timepoints post infection, cells and supernatant were collected for RNA
414 extraction. Infection of undifferentiated 3D-HIEs followed the same protocol with HIEs
415 always cultured in OGM, including the infection medium.
416
417 **HEV infection in transwells**

418 3D-HIEs in OGM were collected and dispersed into single cells with TrypLE express
419 (Gibco) and seeded on semipermeable transwell inserts (0.4 µm PET membrane,
420 VWR) that were precoated with collagen type IV (EMD Millipore). After 2 days in OGM,
421 cells were maintained in ODM until formation of a polarized monolayer (6-7 days).
422 TEER of monolayers was measured using an epithelial voltohmmeter (EVOM, WPI).
423 Polarized monolayers were infected with HEV Kernow-p6-G1634R (2.0×10^8 copies)
424 through the apical side for 6h at 37°C. After, cells were washed five times with CMGF
425 (-). ODM containing 500 µM GCDCA and 2 µM ruxolitinib was added to apical and
426 basal compartments and incubated at 37°C with 5% CO_2. Supernatant from the apical
427 and basolateral sides, and cells from apical side were harvested at multiple time points
428 pi. Infection of undifferentiated 2D-HIE monolayers followed the same protocol with
429 HIEs always cultured in OGM, including the infection medium.
430
431 **Enteroids electroporation**
432 HIE culture and preparation of single cell suspension was performed as described
433 previously[29]. Briefly, 3D-HIEs were kept in OGM for 5 days. Forty eight hours prior to
434 electroporation, medium was replaced by ODM supplemented with 5 µM CHIR99021
435 (StemCell technologies) and 10 µM Y-27632. Twenty four hours prior to electroporation,
436 medium was replaced by ODM supplemented with 5 µM CHIR99021, 10 µM Y-27632
437 and 1.25% (V/V) DMSO. HIE single cell suspensions were prepared with TrypLE
438 express supplemented with 10 µM Y-27632 for 20 min at 37°C.
439 Single-cell suspensions of HIEs (1.0×10^6 cells) were resuspended in 200 µL BTX
440 buffer (BTXpress; BTX Harvard Apparatus), mixed with 10 µg capped Kernow-C1 p6,
441 Kernow-C1 p6-G1634R, Kernow-C1 p6/luc, Kernow-C1 p6 G1634R/luc, pLA-B350/luc,
442 or Sar55/S17/luc RNA in a 4-mm (VWR International) cuvette. An ECM 830 Electro
443 Square Porator™ (BTX Harvard Apparatus) was used to deliver 2 pulses at 450 V, 2
444 msec, 2 pulses with 100 ms intervals between each pulse. The addition of viral RNA
445 to the electroporation mixture was omitted for the cell control samples. Immediately
446 after the electroporation, the cells were transferred to a falcon tube containing 1.5 mL
447 of ODM with 10 µM Y-27632 and incubated at RT for 40 min. After, cells were
448 centrifuged, resuspended in 100% matrigel and plated in pre-warmed 48-well plates
449 (20 µL drop containing 1.0×10^5 cells). For immunofluorescence experiments,
450 electroporated cells were resuspended in 50% matrigel-ODM solution and plated in
451 black wall 96-well plates (Greiner) pre-coated with 5% matrigel. Electroporated cells

452 were cultured in ODM supplemented with 10 µM Y-27632 (10 µM), 5 µM CHIR99021
453 (StemCell technologies) and 1.25% V/V DMSO), with or without ribavirin (Sigma-
454 Aldrich).
455
456 **Luminescence-based replicon assay**
457 To track the replication kinetics of luciferase expression activities in enteroids
458 electroporated with HEV replicons carrying the luciferase gene, 20 µL of culture
459 medium was collected at various time points post-electroporation (day 1 to 11).
460 Luciferase activity was assessed via the Renilla luciferase kit (Promega). In brief, 20
461 µL of the culture medium was transferred to white 96-well Culture Plates (PerkinElmer),
462 followed by the addition of 50 µL (1:100 diluted) *Gaussia* substrate. Luminescence
463 produced by the secreted *Gaussia* luciferase was measured using a Spark microplate
464 reader (Tecan).
465
466 **Cell viability**
467 Enteroid viability was assessed with Live-Dead Cell Viability Assay Kit (EMD Millipore)
468 according to the manufacturer instructions. Briefly, media was aspirated and replaced
469 with dye mixture and incubate for 60 min at 37°C. Images were acquired on DMi8
470 (Leica) fluorescence microscope with a 10x objective.
471
472 **RNA extraction and real-time quantitative PCR (RT-qPCR)**
473 Extracellular viral RNA was extracted from 50 or 150 µL supernatant collected from
474 infected/transfected HIEs or HepG2/C3A cells, by using the NucleoSpin RNA virus kit
475 (Macherey-Nagel). For intracellular viral RNA cells were harvested in TRI Reagent and
476 RNA extraction (Zymo Research, R2051) was performed according to manufacturer's
477 instructions. The HEV RNA loads were quantified using an established human HEV
478 RT- qPCR protocol as previously described[40,41].
479
480 **Immunofluorescence staining and focus-forming assay**
481 Immunofluorescence assays were performed at the peak of replication, *e.g.* after 11
482 days pe, as described previously[23]. Briefly, supernatant was removed without
483 disturbing the HIE layer and cells were fixated with a 2% PFA solution at 4°C overnight.
484 Then cells were permeabilized, blocked and incubated with primary antibodies. The
485 following antibodies were used: anti-ORF2 (HEV-specific rabbit hyperimmune serum),

anti-Ki67 (EMD Millipore, MAB4190), anti-sucrose isomaltase (Santa Cruz Biotechonology, sc-393424), anti-chromogranin A (Santa Cruz Biotechonology, sc-393941), phalloidin (Invitrogen, A12380) or wheat germ agglutinin (WGA, Vector laboratories, RL-1022). Subsequently, cells were incubated with correspondent secondary antibodies (Invitrogen) and nuclear counterstaining for 1h at RT. Images were acquired on an Andor Dragonfly 200 series High Speed confocal platform system (Oxford instruments, Abingdon, UK) at a 25x magnification connected to a Leica DMi8 (Leica Microsystems, Wetzlar, Germany). Image processing was done with the Imaris analysis software (version 9.8.2). The 3D colocalization analysis of virus and intestinal epithelial cell markers was done using Imaris 3D colocalization software (voxel-based colocalization). Images are presented as maximum projections.

For detecting HEV ORF2 in HepG2/C3A cells infected with HEV stocks, cells were fixed on 7 dpi with 3.7 % of PFA and incubated for 30 min at RT. Next, cells were permeabilized with 0.1% Triton X-100, incubated for 30 min at RT, followed by blocking with 3% bovine serum albumin (BSA). Subsequently, the cells were incubated overnight at 4°C with primary antibody anti-ORF2 (HEV-specific rabbit hyperimmune serum), after which incubated with a secondary antibody goat anti-rabbit Alexa Fluor 488 (1:800, Thermo Scientific) for 1h. The nuclei were labelled with DAPI (1:1000 dilution; Sigma).

HepG2/C3A cells (7500 cells/well) were seeded in a 96-well plate with 10% complete DMEM the day prior to HEV infection. Viruses were serially diluted at 1:3, with a 1:6 dilution as the starting dilution. On the 7 dpi, the 96-well plate was fixed for immunofluorescence assay (IFA), and fluorescence images of each well were acquired using a high-content imager (Arrayscan XTI, Thermo Fisher Scientific). Viral titers were determined by counting the number of focus-forming units (FFU) containing HEV ORF2-positive cells through image analysis using the HCS Studio Cellomics software (Thermo Fisher Scientific, Version 6.6.2).

Statistical analysis

All statistical analyses were performed using the GraphPad Prism 10.2.0 software (GraphPad Software, Inc.).

Acknowledgements

We thank Prof. Luc Verschaeve (formerly at the Scientific Institute of Public Health, Brussels, Belgium), Prof. Jason Spence (University of Michigan Medical School) and Prof. Mary Estes (University of Michigan Medical School) for proving the HepG2/C3A cells, fetal ileum HIEs and adult jejunum HIEs, respectively. We also thank Prof. Eike Steinmann (Ruhr University Bochum, Germany) for the anti-ORF2 HEV-specific rabbit hyperimmune serum.

Financial support

This work was supported by the Horizon 2020-funded ITN program OrganoVIR (Grant 812673); and the KU Leuven Starting Grant STG/21/028 to JRP. XZ was supported by the China Scholarship Council (grant no. 201906170033).

References

1. Purdy, M. A. *et al.* ICTV Virus Taxonomy Profile: Hepeviridae 2022. *J. Gen. Virol.* **103**, 1–2 (2022).
2. Raji, Y. E., Toung, O. P., Taib, N. M. & Sekawi, Z. Bin. Hepatitis E Virus: An emerging enigmatic and underestimated pathogen. *Saudi J. Biol. Sci.* **29**, 499–512 (2022).
3. Rein, D. B., Stevens, G. A., Theaker, J., Wittenborn, J. S. & Wiersma, S. T. The global burden of hepatitis E virus genotypes 1 and 2 in 2005. *Hepatology* **55**, 988–997 (2012).
4. Chaudhry, S. A., Verma, N. & Koren, G. Hepatitis e infection during pregnancy. *Can. Fam. Physician* **61**, 607–608 (2015).
5. Fousekis, F. S., Mitselos, I. V. & Christodoulou, D. K. Extrahepatic manifestations of hepatitis E virus: An overview. *Clin. Mol. Hepatol.* **26**, 16–23 (2020).
6. Ma, Z., de Man, R. A., Kamar, N. & Pan, Q. Chronic hepatitis E: Advancing research and patient care. *J. Hepatol.* **77**, 1109–1123 (2022).
7. Mesquita, J. R., Myrmel, M., Stene-Johansen, K., Øverbø, J. & Nascimento, M. S. J. A Public Health initiative on hepatitis E virus epidemiology, safety and control in Portugal - study protocol. *BMC Infect. Dis.* **16**, 1–5 (2016).
8. Debing, Y. *et al.* A mutation in the hepatitis e virus RNA polymerase promotes its replication and associates with ribavirin treatment failure in organ transplant recipients. *Gastroenterology* **147**, 1008-1011.e7 (2014).

553 9. Todt, D., Walter, S., Brown, R. J. P. & Steinmann, E. Mutagenic effects of
554 ribavirin on hepatitis E virus-viral extinction versus selection of fitness-
555 enhancing mutations. *Viruses* **8**, 1–15 (2016).
556 10. Debing, Y. *et al.* Hepatitis E virus mutations associated with ribavirin treatment
557 failure result in altered viral fitness and ribavirin sensitivity. *J. Hepatol.* **65**,
558 499–508 (2016).
559 11. Meister, T. L., Bruening, J., Todt, D. & Steinmann, E. Cell culture systems for
560 the study of hepatitis E virus. *Antiviral Res.* **163**, 34–49 (2019).
561 12. Kamar, N. *et al.* Hepatitis E virus infection. *Nat Rev Dis Prim.* **16**, 1–16 (2017).
562 13. Takahashi, M. *et al.* Monoclonal antibodies raised against the ORF3 protein of
563 hepatitis e virus (HEV) can capture HEV particles in culture supernatant and
564 serum but not those in feces. *Arch. Virol.* **153**, 1703–1713 (2008).
565 14. Yin, X., Ambardekar, C., Lu, Y. & Feng, Z. Distinct Entry Mechanisms for
566 Nonenveloped and Quasi-Enveloped Hepatitis E Viruses. *J. Virol.* **90**, 4232–
567 4242 (2016).
568 15. Todt, D. *et al.* Robust hepatitis e virus infection and transcriptional response in
569 human hepatocytes. *Proc. Natl. Acad. Sci. U. S. A.* **117**, 1731–1741 (2020).
570 16. Takahashi, M. *et al.* Hepatitis e virus (HEV) strains in serum samples can
571 replicate efficiently in cultured cells despite the coexistence of HEV antibodies:
572 Characterization of HEV virions in blood circulation. *J. Clin. Microbiol.* **48**,
573 1112–1125 (2010).
574 17. Marion, O. *et al.* Hepatitis e virus replication in human intestinal cells. *Gut* **69**,
575 901–910 (2020).
576 18. Li, P. *et al.* Recapitulating hepatitis E virus-host interactions and facilitating
577 antiviral drug discovery in human liver-derived organoids. *Sci. Adv.* **8**, 1–17
578 (2022).
579 19. Estes, M. K. *et al.* Human Norovirus Cultivation in Nontransformed Stem Cell-
580 Derived Human Intestinal Enteroid Cultures: Success and Challenges. *Viruses*
581 **11**, 9–11 (2019).
582 20. Saxena, K. *et al.* Human Intestinal Enteroids: a New Model To Study Human
583 Rotavirus Infection, Host Restriction, and Pathophysiology. *J. Virol.* **90**, 43–56
584 (2016).
585 21. Kolawole, A. O. *et al.* Astrovirus replication in human intestinal enteroids
586 reveals multi-cellular tropism and an intricate host innate immune landscape.

587 *PLoS Pathog.* **15**, 1–30 (2019).
588 22. Holly, M. K. & Smith, J. G. Adenovirus Infection of Human Enteroids Reveals
589 Interferon Sensitivity and Preferential Infection of Goblet Cells. *J. Virol.* **92**, 1–
590 15 (2018).
591 23. Masmoudi, F. *et al.* Evaluation of 3D Human Intestinal Organoids as a
592 Platform for EV-A71 Antiviral Drug Discovery. *Cells* **12**, 1–14 (2023).
593 24. Sato, T. *et al.* Single Lgr5 stem cells build crypt-villus structures in vitro without
594 a mesenchymal niche. *Nature* **459**, 262–265 (2009).
595 25. Günther, C., Winner, B., Neurath, M. F. & Stappenbeck, T. S. Organoids in
596 gastrointestinal diseases: From experimental models to clinical translation. *Gut*
597 **71**, 1892–1908 (2022).
598 26. Taelman, J., Diaz, M. & Guiu, J. Human Intestinal Organoids: Promise and
599 Challenge. *Front. Cell Dev. Biol.* **10**, 1–9 (2022).
600 27. Mirabelli, C. *et al.* Human Norovirus Efficiently Replicates in Differentiated 3D-
601 Human Intestinal Enteroids. *J. Virol.* **96**, (2022).
602 28. Santos-Ferreira, N. *et al.* Molnupiravir inhibits human norovirus and rotavirus
603 replication in 3D human intestinal enteroids. *Antiviral Res.* **223**, (2024).
604 29. Fujii, M., Matano, M., Nanki, K. & Sato, T. Efficient genetic engineering of
605 human intestinal organoids using electroporation. *Nat. Protoc.* **10**, 1474–1485
606 (2015).
607 30. Wang, F. *et al.* Isolation and characterization of intestinal stem cells based on
608 surface marker combinations and colony-formation assay. *Gastroenterology*
609 **145**, 383–395 (2013).
610 31. Shukla, P. *et al.* Adaptation of a Genotype 3 Hepatitis E Virus to Efficient
611 Growth in Cell Culture Depends on an Inserted Human Gene Segment
612 Acquired by Recombination. *J. Virol.* **86**, 5697–5707 (2012).
613 32. Lemon, S. M. & Walker, C. M. Enterically transmitted non-a, non-b hepatitis
614 and the discovery of hepatitis E virus. *Cold Spring Harb. Perspect. Med.* **9**, 1–
615 14 (2019).
616 33. Blutt, S. E. & Estes, M. K. Organoid Models for Infectious Disease. *Annu. Rev.*
617 *Med.* **73**, 167–182 (2022).
618 34. Stewart, C. E., Rall, R. E. & Adamson, C. S. Inhibitors of the interferon
619 response enhance virus replication in vitro. *PLoS One* **9**, 3–10 (2014).
620 35. Kong, F., Saif, L. J. & Wang, Q. Roles of bile acids in enteric virus replication.

621 *Anim. Dis.* **1**, 1–9 (2021).
622 36. Latorre, R., Sternini, C., De Giorgio, R. & Greenwood-Van Meerveld, B.
623 Enteroendocrine cells: A review of their role in brain-gut communication.
624 *Neurogastroenterol. Motil.* **28**, 620–630 (2016).
625 37. Emerson, S. U. *et al.* Recombinant hepatitis E virus genomes infectious for
626 primates: Importance of capping and discovery of a cis-reactive element. *Proc.*
627 *Natl. Acad. Sci. U. S. A.* **98**, 15270–15275 (2001).
628 38. Debing, Y. *et al.* A rat model for hepatitis E virus. *DMM Dis. Model. Mech.* **9**,
629 1203–1210 (2016).
630 39. Meister, T. L., Klöhn, M., Steinmann, E. & Todt, D. A cell culture model for
631 producing high titer hepatitis e virus stocks. *J. Vis. Exp.* **2020**, 1–19 (2020).
632 40. Debing, Y. *et al.* Ribavirin inhibits in vitro hepatitis E virus replication through
633 depletion of cellular GTP pools and is moderately synergistic with alpha
634 interferon. *Antimicrob. Agents Chemother.* **58**, 267–273 (2014).
635 41. Zhang, X. *et al.* Establishment of a robust rat hepatitis E virus fecal-oral
636 infection model and validation for antiviral studies. *Antiviral Res.* **216**, 105670
637 (2023).
638
639

640 **Figure 1**

641

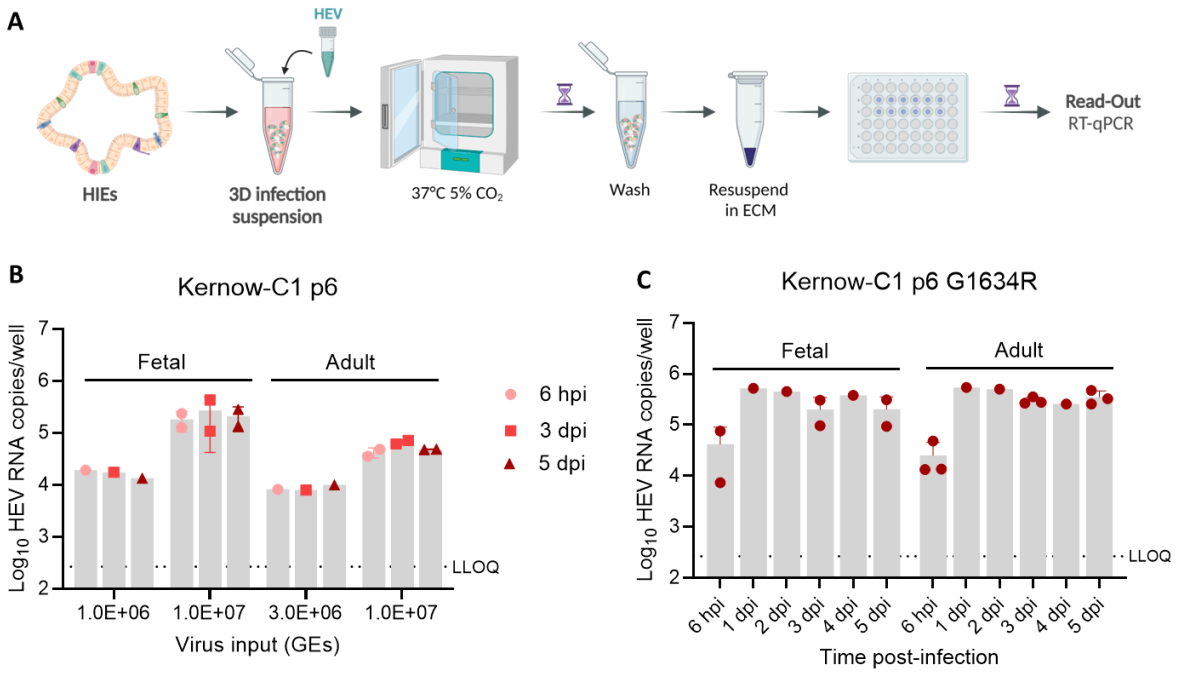

642

643

644 **Figure 1 – HEV replication in 3D-HIEs. (A)** Schematic representation of the
645 experimental layout. **(B)** Fetal and adult differentiated 3D-HIEs were infected with
646 increasing inputs of HEV Kernow-C1 p6 (env$^-$) (N=2). **(C)** Fetal (N=2) or adult (N=3)
647 differentiated 3D-HIEs were infected with HEV Kernow-C1 p6 (env$^-$) 5.0 × 10^7 GEs.
648 Infection medium was supplemented with GCDCA and ruxolitinib. Intracellular and
649 extracellular HEV RNA was quantified by RT-qPCR. The dotted line represents the
650 LLOQ (lower limit of quantification). Data are presented as mean ± SD. GEs – genome
651 equivalents. Figure created with BioRender.com.

652

653

654

655

656

657

658

659

660

661

662

663

664 **Figure 2**

665

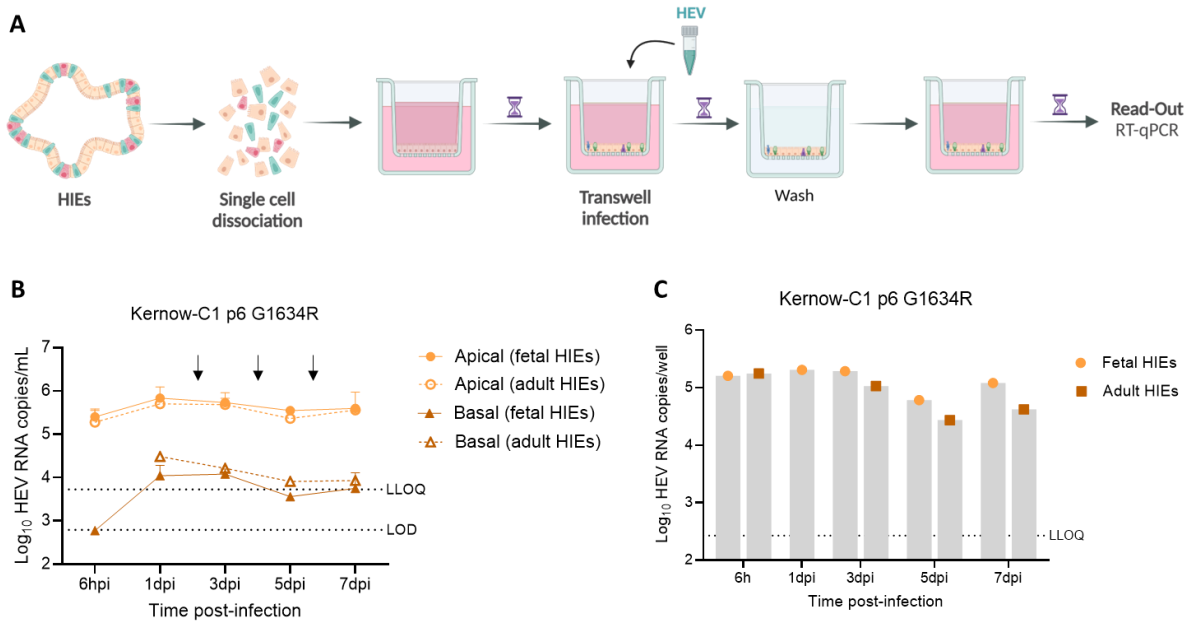

666

667

668 **Figure 2 – HEV replication in polarized HIEs in a transwell system. (A)** Schematic
669 representation of the experimental layout. **(B)** Extracellular HEV released into apical
670 or basal supernatant of fetal (N=2) or adult (N=1) differentiated 2D-HIEs infected with
671 HEV Kernow-C1 p6 G1634R (env$^-$) (2.0 × 10^8 copies). Half of the medium (100 µL
672 apical and 300 µL basolateral compartment) was refreshed every 2 days (black
673 arrows). **(C)** Intracellular HEV RNA levels in fetal or adult differentiated 2D-HIEs cell
674 lysates. HEV RNA was quantified by RT-qPCR. The dotted line represents the LLOQ
675 (lower limit of quantification) or the LOD (limit of detection). Data are presented as
676 mean ± SD. Figure created with BioRender.com.

677

678

679

680

681

682

683

684

685

686 **Figure 3**

687

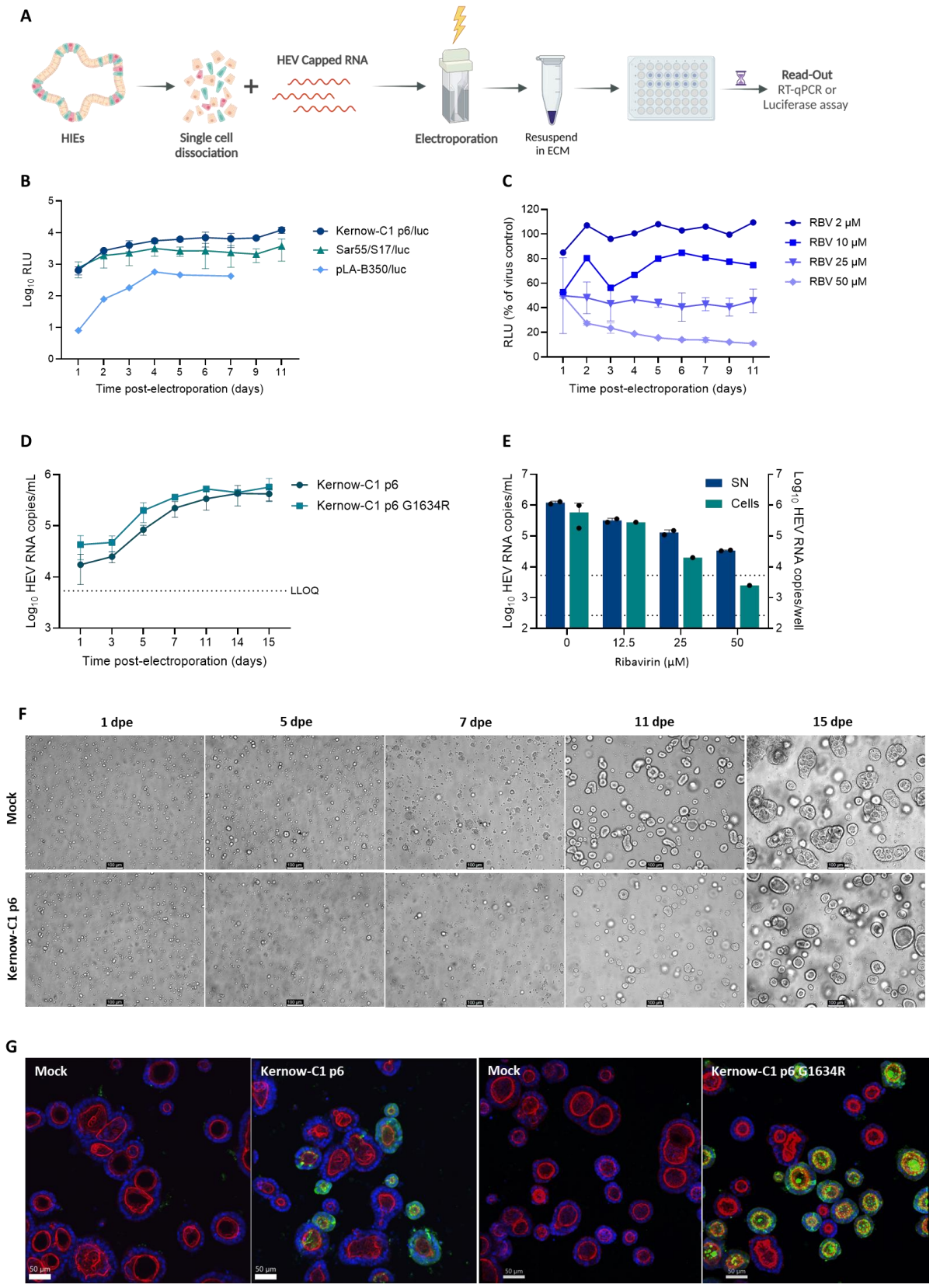

688
689
690

691 **Figure 3 – Electroporated HIEs are permissive to HEV replication.** (A) Schematic
692 representation of the experimental layout. (B) Fetal HIEs were electroporated with
693 mock, HEV-3 Kernow-C1 p6/luc (N=2), HEV-1 Sar55/S17/luc (N=2) or ratHEV pLA-
694 B350/luc (N=1) capped RNA. (C) HEV-3 Kernow-C1 p6/luc electroporated HIEs were
695 treated with increasing concentrations of ribavirin (RBV) (N=2) up to 11 days post-
696 electroporation (pe). Viral replication related luciferase activity was determined in 20
697 µL supernatant (extracellular HEV) up to 11 days pe. (D) Fetal HIEs were
698 electroporated with mock, HEV-3 Kernow-C1 p6 (N=3) or Kernow-C1 p6 G1634R (N=2)
699 full-length capped RNA. Half medium was refreshed at 11 days pe. Viral replication
700 was determined by RT-qPCR in 50 µL supernatant (extracellular HEV) up to 15 days
701 pe. (E) HEV-3 Kernow-C1 p6 G1634R electroporated HIEs were treated with
702 increasing concentrations of ribavirin (RBV) (N=1). Viral load was determined at 13
703 days pe by RT-qPCR in HIE cells (intracellular HEV) or in 50 µL supernatant
704 (extracellular HEV). (F) Light microscopy of mock and Kernow-C1 p6 electroporated
705 fetal HIEs up to 15 days pe. Images acquired on DMi8 microscope (Leica) using a 10x
706 objective. Scale bar – 100 µm. (G) Representative images of HEV ORF2 expression
707 in Kernow-C1 p6 or Kernow-C1-p6 R electroporated fetal HIEs at 15 days pe.
708 Immunofluorescence staining with ORF2 (green) – HEV; Phalloidin (red) – actin; and
709 DAPI (blue) – Nuclei. Images acquired on Spinning-disk confocal with a 25x objective.
710 Scale bar – 50 µm. RLU, relative luminescence units. Dpe – days post-electroporation.
711 Data are presented as mean ± SD. The dotted line represents the LLOQ of the
712 intracellular or extracellular. Figure created with BioRender.com.
713
714
715
716
717
718
719
720
721
722
723
724

725 **Figure 4**

726

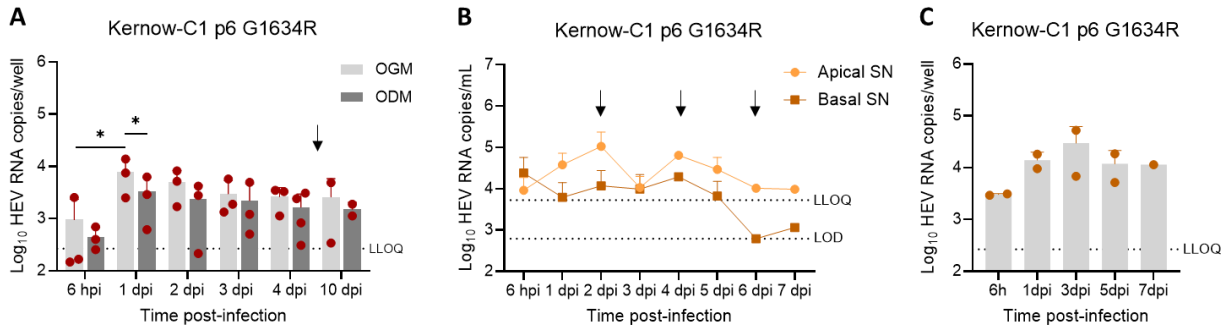

727

728

729

730 **Figure 4 – HEV replication in proliferating fetal HIEs. (A)** Proliferating (OGM) and
731 differentiated (ODM) fetal 3D-HIEs were infected with HEV Kernow-C1 p6 G1634R
732 ($env^{+/-}$) 3.0 × 10^7 GEs (N=3). Medium was supplemented with GCDCA and ruxolitinib.
733 Half infection medium (300 µL) was replaced every 2 days starting from day 4 post-
734 infection (pi) (black arrow). Intracellular and extracellular HEV RNA was quantified by
735 RT-qPCR. Data are presented as mean ± SD. **(B)** Proliferating fetal 2D-HIEs in
736 transwells were infected with HEV Kernow-C1 p6 G1634R (env^{-}) 2.0 × 10^8 GEs (N=2).
737 Extracellular HEV released into apical or basal supernatant was quantified. Half
738 medium (100 µL apical and 300 µL basolateral compartment) was refreshed every 2
739 days (black arrows). **(C)** Intracellular HEV RNA in proliferating 2D-HIE cell lysates.
740 HEV RNA was quantified by RT-qPCR. The dotted line represents the LLOQ (lower
741 limit of quantification) or the LOD (limit of detection). Data are presented as mean ±
742 SD. *, $P < 0.05$. Student's t test.

743

744

745

746

747

748

749

750

751

752

753 **Figure 5**

754

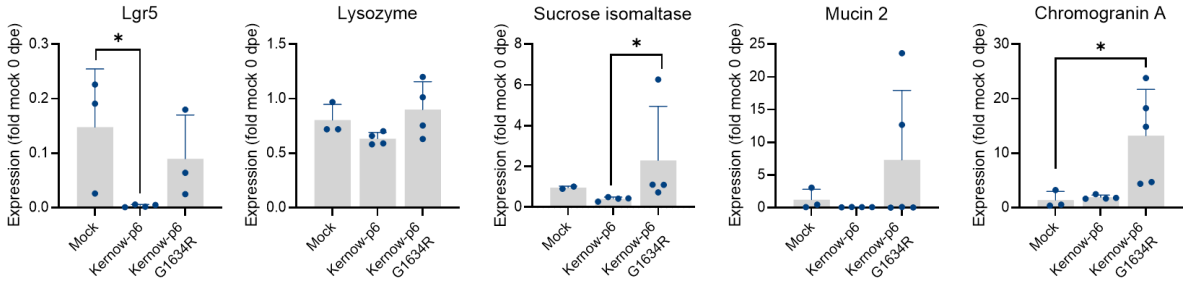

755

756

757 **Figure 5 – HIE intestinal epithelial cell expression upon electroporation with HEV**
758 **RNA.** Stem cells (LGR5+), Paneth cells (lysozyme), enterocytes (sucrose isomaltase),
759 goblet cells (MUC2) and enteroendocrine cells (chromogranin A) gene expression in
760 mock-, Kernow-C1 p6 (N=1) or Kernow-C1 p6 G1634R (N=3) electroporated fetal
761 HIEs at 11 days post electroporation (dpe). mRNA levels of selected host genes were
762 quantified by RT-qPCR. Cell number was normalized with GADPH gene. Fold change
763 is relative to mock HIEs at 0 dpe. *, $P < 0.05$. Kruskal-Wallis test.

764

765

766

767

768

769

770

771

772

773

774

775

776

777

778

779

780

781

782 **Figure 6**

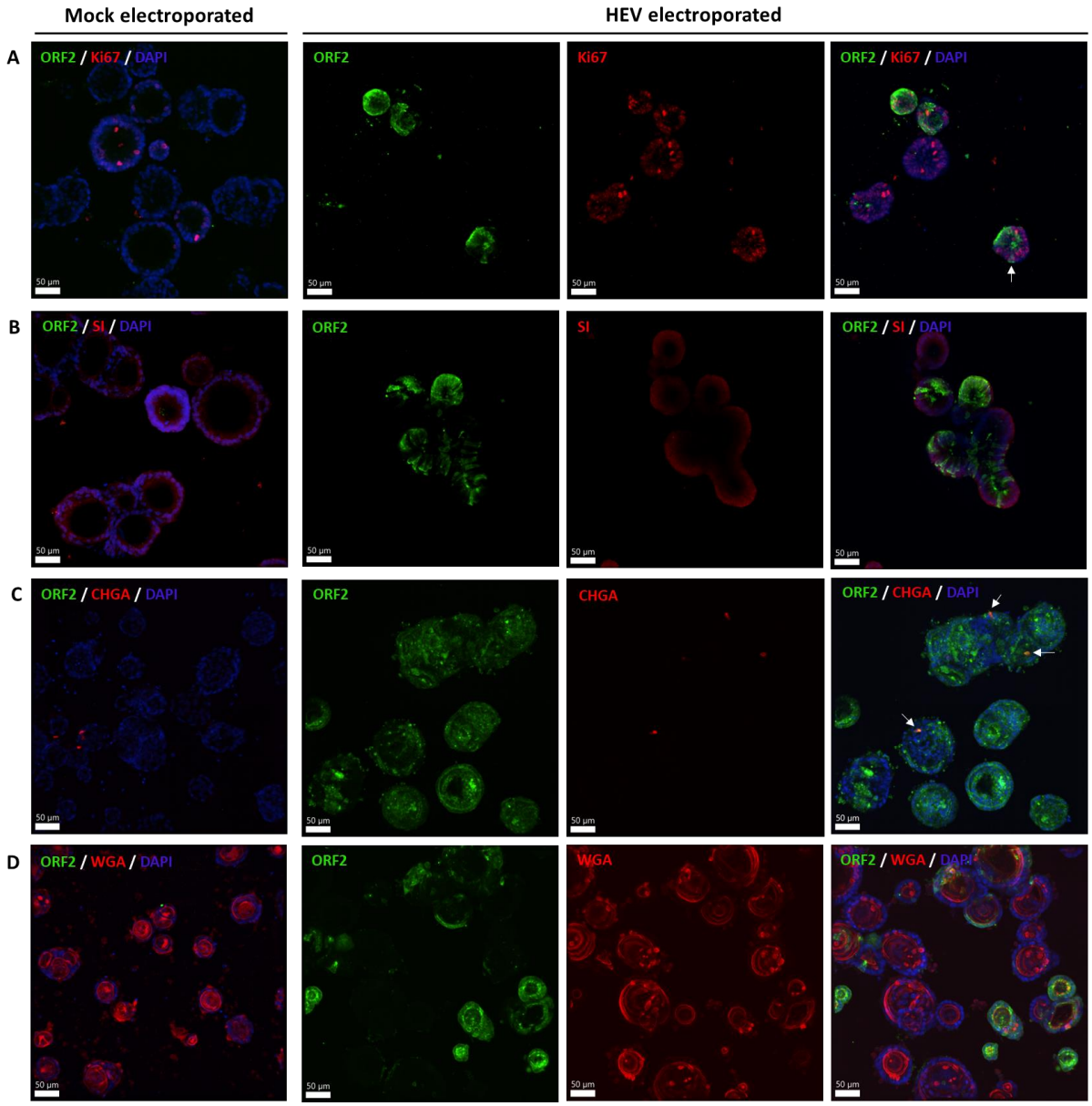

783

784

785 **Figure 6 – HEV tropism in human intestinal epithelial cells.** Representative images
786 of immunofluorescence staining of Kernow-C1 p6 or Kernow-C1 p6 G1634R
787 electroporated fetal HIEs at 11 days pe stained with HEV ORF2-specific antibody
788 (green) and specific antibody for **(A)** proliferating cells (Ki67), **(B)** enterocytes (SI -
789 sucrose isomaltase), **(C)** enteroendocrine cells (CHGA - chromogranin A) or **(D)** goblet
790 cells (WGA – wheat germ agglutinin). Mock electroporated HIEs were included as
791 negative control. DAPI (blue) was used as counterstaining (nuclei) ORF2 (green).
792 Scale bar – 50 µm.

793

794 **Supplementary figure 1**

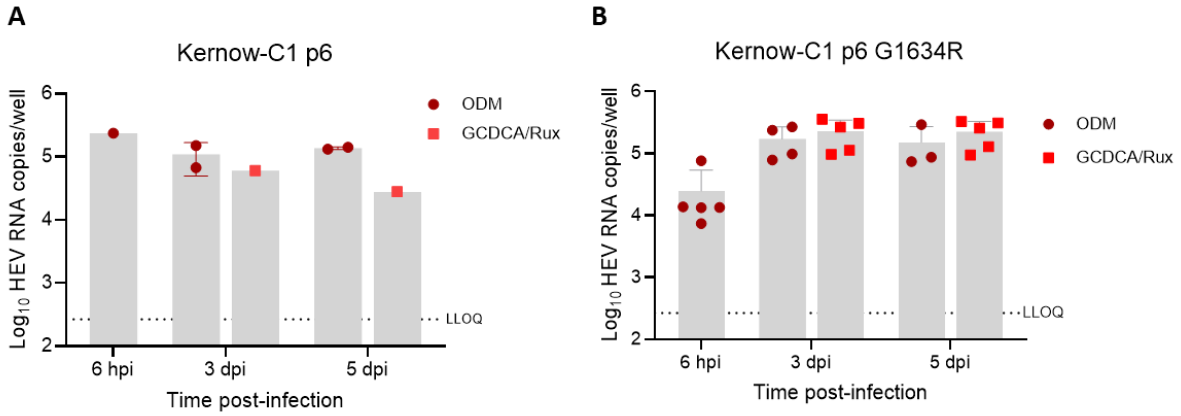

795

796

797 **Figure S1 – Effect of GCDCA and ruxolitinib in HEV replication.** (A) Fetal
798 differentiated 3D-HIEs were infected with Kernow-C1 p6 (env-) 1.0 × 107 GEs (N=2).
799 (B) Differentiated 3D-HIEs (data from fetal and adult HIEs was combined) were
800 infected with Kernow-C1 p6 G1634R (env-) 5.0 × 107 GEs (N=4). Intracellular and
801 extracellular HEV RNA was quantified by RT-qPCR. Data are presented as mean ±
802 SD. GEs – genome equivalents.

803

804

805

806 **Supplementary figure 2**

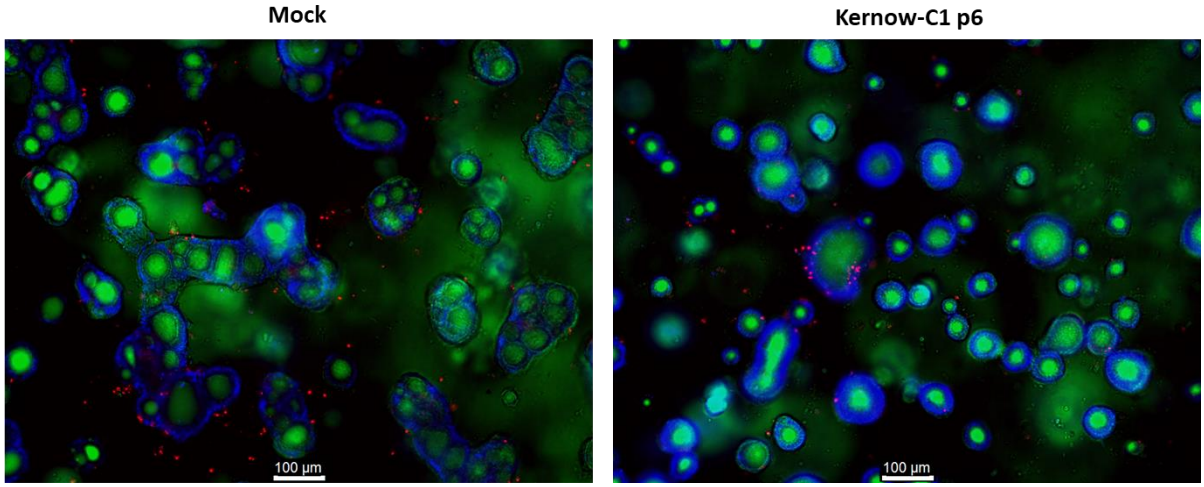

807

808 **Figure S2 – Representative images of live-dead cell viability assay of mock or**
809 **HEV Kernow-C1 p6 electroporated fetal HIEs at 15 days pe.** Calcein-AM (green),
810 propidium iodide (red) and Hoechst 33342. Images acquired on DMi8 (Leica) with a
811 10x objective. Scale bar – 100 µm.

812

813 **Supplementary figure 3**

814

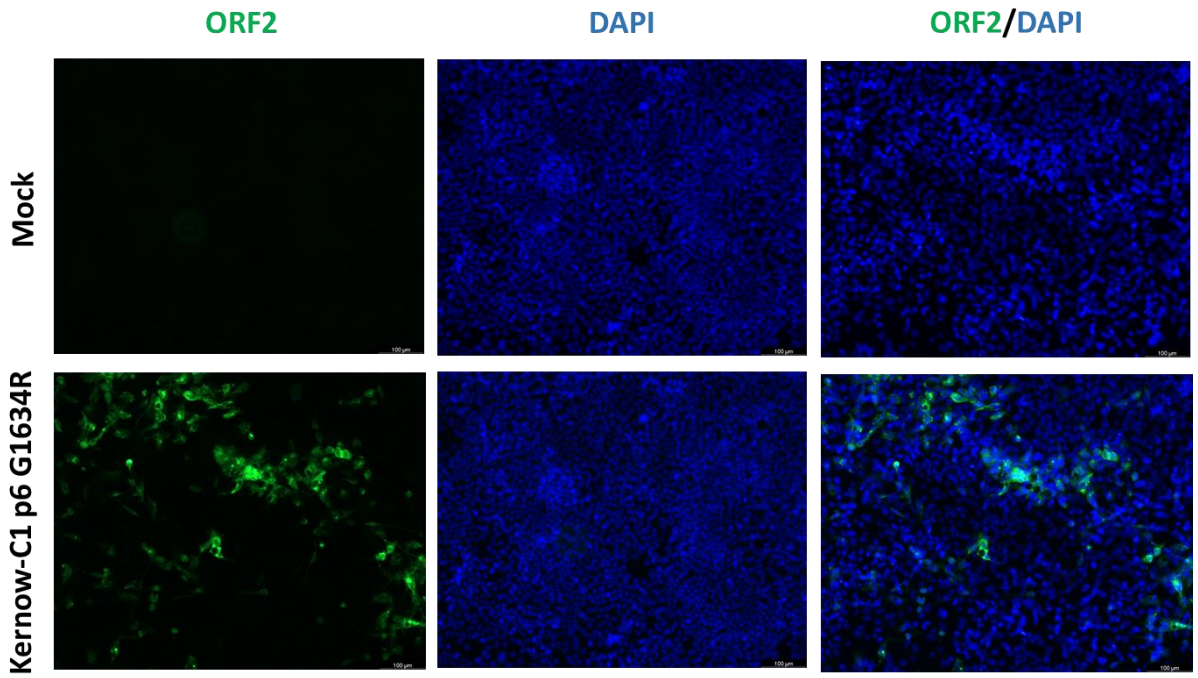

815

816 **Figure S3 - Immunofluorescence staining of HEV ORF2 in HepG2/C3A cells**
817 **infected with supernatant of Kernow-C1 p6 G1634R electroporated HIEs (1:6**
818 **dilution).** Uninfected HepG2/C3A cells were included as negative control. Scale bar
819 – 100 µm. Green = ORF2; Blue = DAPI. Images acquired on DMi8 (Leica) with a 10x
820 objective.

821

822

823

824

825

826

827

828

829

830

831

832

833

834 **Supplementary figure 4**

835

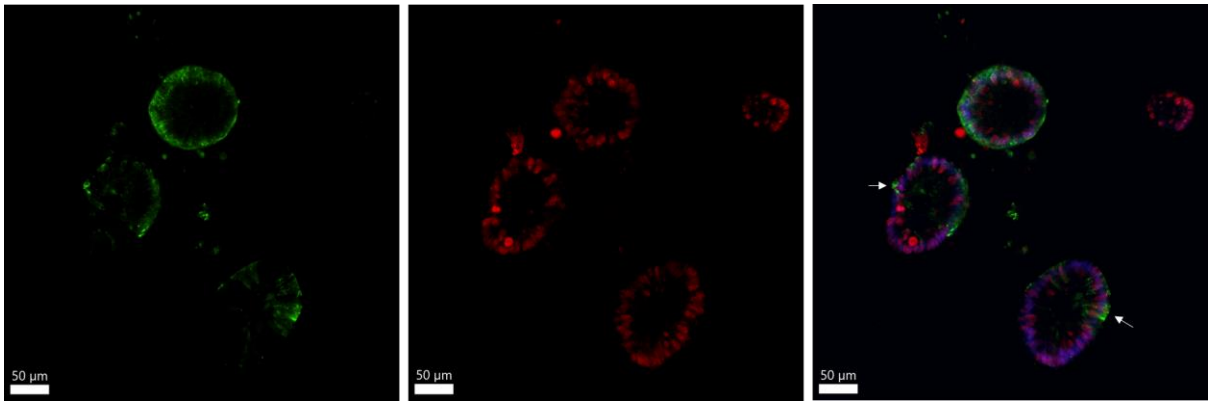

836

837

838 **Figure S4 - Immunofluorescence staining of HEV ORF2 and proliferating cells**
839 **upon Kernow-C1 p6 G1634R infection in HIEs.** The HEV ORF2 (green) and
840 proliferating cells (Ki67, red) are visualized in Kernow-C1 p6 G1634R electroporated
841 HIEs at 11 days pe. Counterstaining with DAPI (nuclei, blue). Scale bar – 50 µm.

842

843

844

845 **Supplementary figure 5**

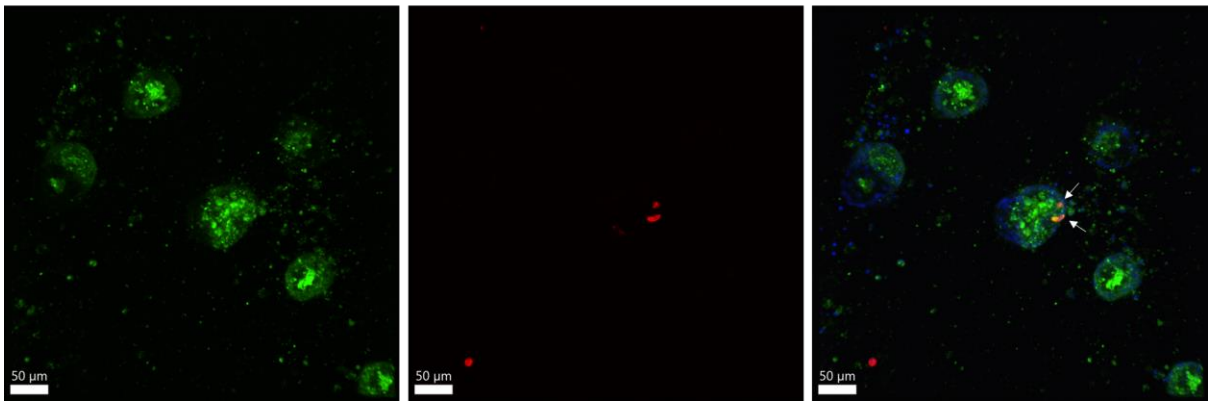

846

847 **Figure S5 - Immunofluorescence staining of HEV ORF2 and enteroendocrine**
848 **cells upon Kernow-C1 p6 G1634R infection in HIEs.** The HEV ORF2 (green) and
849 enteroendocrine cells (chromogranin A, red) are visualized in Kernow-C1 p6 G1634R
850 electroporated HIEs at 11 days pe. Counterstaining with DAPI (nuclei, blue). Scale bar
851 – 50 µm.

852